applied sciences

MDPI

Article

Transient Response of Dynamic Stress Concentration around a Circular Opening: Incident SH Wave

Jiayou Weng [1], Zhiwen Wang [1,*], Chuanping Zhou [1], Wanrong Pei [1], Rougang Zhou [1,2,*], Rong Liu [1] and Yongping Gong [1,3]

[1] School of Mechanical Engineering, Hangzhou Dianzi University, Hangzhou 310018, China; joany0204@163.com (J.W.); zhoucp@hdu.edu.cn (C.Z.); wrpei@hdu.edu.cn (W.P.); 40471@hdu.edu.cn (R.L.); gyp@hdu.edu.cn (Y.G.)
[2] Wenzhou Institute, Hangzhou Dianzi University, Wenzhou 325000, China
[3] School of Mechanical Engineering, Zhejiang University, Hangzhou 310062, China
* Correspondence: wzw3049972460@hdu.edu.cn (Z.W.); 42141@hdu.edu.cn (R.Z.)

Abstract: The present study aims to investigate the transient response of stress concentration around a circular opening. The study focuses on the composition of the shockwave, which consists of SH waves of multiple frequencies. The wave equation, expressed by the displacement function, is transformed into the Helmholtz equation through the Fourier transform method. The spectral function can be obtained by employing analytic continuation and Fourier transform of the incident wave field. An analytical expression for the dynamic stress around the aperture can be derived using the wave function expansion method and by considering the boundary conditions. The influence of the aperture on the transient response is discussed based on the distribution of the dynamic stress concentration coefficient and stress peak coefficient under different aperture sizes. The results show that the peak of the dynamic stress concentration coefficient changes with the aperture. In contrast, the stress peak coefficient is primarily concentrated in the early stages of the transient response. Furthermore, it is observed that larger radii can induce alternating stress in the material, which may lead to fatigue failure. This strategy provides a solution for addressing similar challenges.

Keywords: SH wave; dynamic stress concentration; transient corresponding; Fourier transform; wave function expansion method

Citation: Weng, J.; Wang, Z.; Zhou, C.; Pei, W.; Zhou, R.; Liu, R.; Gong, Y. Transient Response of Dynamic Stress Concentration around a Circular Opening: Incident SH Wave. *Appl. Sci.* **2023**, *13*, 9824. https://doi.org/10.3390/app13179824

Academic Editor: Angelo Luongo

Received: 29 July 2023
Revised: 22 August 2023
Accepted: 24 August 2023
Published: 30 August 2023

1. Introduction

The study of elastic wave propagation in continuous media holds significant importance in elastic dynamics. Understanding stress concentration under dynamic conditions is crucial for ensuring the safety and reliability of engineering applications. It plays a pivotal role in seismic design, ore exploration, non-destructive testing, blasting, and the application and advancement of advanced composite materials. Defects such as openings, inclusions, and cracks are often present when manufacturing and processing artificial materials. Consequently, investigating dynamic stress concentration around scattering waves and defects has become a focal point of research [1]. As early as 1973, Pao et al. [2] researched dynamic stress concentration problems associated with various defects. Since then, numerous numerical examples have been provided, and the mechanical properties of materials with defects have emerged as a prominent research area.

In recent decades, the theoretical analysis of elastic wave propagation in continuous media has focused on three key aspects: model structure, defect morphology, and constitutive relationships. Scholars have extensively researched these problem categories [3–7]. For instance, Xue et al. [3] utilized the wave function expansion method based on magneto-acoustic coupling dynamics theory to address the issues of acoustic wave scattering and dynamic stress concentration in e-type piezoelectric composite materials. Kara et al. [4] investigated the dynamic response of a cylindrical shell surrounded by homogeneous, isotropic, and linear elastic media under plane harmonic excitation. Leng et al. [5] studied the scattering of SH waves by two circular cavities in an elastic plate. They derived the incident and scattered conductive waves that meet the stress-free conditions of the upper and lower surfaces within the band domain. This was achieved through a combination of wave function expansion, complex functions, image method, and multipolar coordinate translation techniques. Jiang et al. [6] conducted an analytical study on the scattering problem of horizontal waves in two-dimensional approximately linear inhomogeneous media using the method of complex variables. They proposed a novel transformation method to normalize the governing equations of two-dimensional inhomogeneous media and employed complex variables to represent the wave field and stress. Tang et al. [7] proposed a series solution for cylindrical SH-wave scattering in a shallow asymmetrical V-shaped canyon and studied the effect of source location on terrain amplification. By comparing the data of two published cases (cylindrical SH-wave symmetrical V-shaped canyon and planar SH-wave asymmetric shallow V-shaped canyon), they found that the difference of displacement amplitude between the asymmetric canyon and the symmetric canyon under the action of cylindrical SH wave can reach 270.2%, that is, the asymmetric effect of the canyon has a significant influence on the topography amplification.

With the emergence of functionally graded materials, research on the mechanics of such materials has become indispensable. An et al. [8] proposed a method to evaluate stress concentration near a circular opening at a permeable interface crack tip in exponential-gradient piezoelectric biomaterials. They established a mechanical model of the crack using the crack connection method and derived the dynamic stress intensity factors at the crack tip. Jiang et al. [9] developed a theoretical approach to investigate magnetoelastic coupling waves and dynamic stress intensity around a cylindrical opening in exponential gradient piezoelectric materials. They provided numerical examples of dynamic stress intensity factors near the opening. Baytak and Bulut [10] developed an experimental and numerical model to understand the thermal stress distribution of functionally graded plates with only the coefficient of thermal expansion. The experimental model and numerical model established by them have a certain practicability for a thermal stress analysis of functionally graded plates. Zhou et al. [11] investigated dynamic stress concentration in an infinite exponential-graded material with two openings using complex variable and conformal mapping methods combined with local coordinates and elastic wave scattering. Kumar et al. [12] investigated the effect of porosity distribution on the nonlinear free vibration and transient analysis of a porous functionally graded skew plate with multiple holes. They adopted a modified power law equation to describe the effective material properties of the porous functionally graded skew plate and applied the first-order shear deformation theory and von Karman's nonlinear strain–displacement relationship to derive a nonlinear finite element calculation formula for the overall porous functionally graded skew plate.

The research mentioned above primarily focuses on cases involving infinite planes and circular apertures, while studying non-circular apertures and semi-infinite planes is more practical. An et al. [13] evaluated stress concentration near an eccentric elliptical opening with a penetrable interface crack tip in a piezoelectric material under anti-plane shear loading. They utilized methods such as Green's function and conformal mapping methods to solve the boundary condition problem and analyze the stress concentration near the crack tip. This study provides valuable insights into the behavior of piezoelectric materials under shear loading conditions and the effects of crack geometry on stress concentration. Zhao et al. [14] investigated the influence of different geometric and physical parameters on the dynamic stress intensity factor at the crack tip using methods such as Green's function, complex variables, and multipolar coordinates. They conducted theoretical research on the dynamic debonding of cylindrical inclusions near the interface of a semi-infinite piezoelectric material. Jiang et al. [15] applied the method of complex variables and multipolar coordinate systems to study the dynamic stress concentration coefficient (DSCC) around a cylindrical cavity in a vertically non-uniform half-space. Their study considered a density variation in the half-space while the shear modulus remained constant.

Jiang et al. [16] studied the dynamic response of shallow circular inclusions in a radially non-uniform half-space under SH wave incidence. They considered that the mass density of the half-space varies with the radii, and the governing equation can be expressed as a variable-coefficient Helmholtz equation. It can be observed that methods such as complex variables, Green's function, and multipolar coordinates play a significant role in the study of non-circular apertures.

Although significant research achievements have been made in stress concentration around openings, most of the studies found in the existing literature focuses on the steady-state response of dynamic stress [3–11,17,18]. Currently, few studies provide analytical solutions for the transient response of materials with openings. Panji et al. [19,20] developed a direct time-domain boundary element method for half-planes, which was successfully applied to analyze the transient response of arbitrarily shaped lined tunnels on the ground surface. This model is simple and highly accurate through an analysis and comparison of the existing literature and then applied to alluvial valleys of arbitrary shape propagated by obliquely incident plane SH waves. Zhou and Shui [21] theoretically analyzed the propagation of transient waves in the piezoelectric and magnetic half-space under the action of dynamic anti-plane concentrated linear forces, and obtained explicit closed solutions of transverse displacement, shearing stress, magnetic potential, and induction via Laplace transform and Cagniard de-Hoop method. Experimentally, Tao et al. [22] proposed an experimental method to explore the dynamic failure process of pre-stressed circular opening rock specimens. They demonstrated the failure process of rock specimens under different initial static stresses and dynamic loading coupling effects using high-speed cameras. Shi et al. [23] provided a method for detecting circumferential cracks. They used a periodic permanent magnet electromagnetic acoustic transducer to generate SH_0-guided waves, and established a finite element model of SH_0-guided waves propagating in the pipeline. The relevant information of reflected waves can provide an accurate and quantitative characterization of pipeline defects.

This study aims to propose a practical, theoretical approach to obtain analytical solutions for the dynamic stress around a circular aperture. We will present numerical results and discuss the stress distribution at the edge of the aperture at the moment of maximum stress occurrence, as well as the influence of the radii on the distribution of dynamic stress. It plays an important role in seismic design, mineral exploration, nondestructive testing, blasting, and the application and progress of advanced composite materials.

2. Governing Equations

Consider the anti-plane governing equation [13] in the cylindrical coordinate system (r, θ, z), where the z-axis is the polarization direction, as the result is

$$\frac{\tau_{rz}}{r} + \frac{\partial \tau_{rz}}{\partial r} + \frac{1}{r}\frac{\partial \tau_{\theta z}}{\partial \theta} = \rho \frac{\partial^2 w^*}{\partial t^2}, \tag{1}$$

where τ_{rz} and $\tau_{\theta z}$ are the shear stress, w^* is the field function of the elastic wave, and ρ is the mass density.

The constitutive relation of the material can be expressed as [11]:

$$\begin{aligned} \tau_{rz} &= \mu \frac{\partial w^*}{\partial r}, \\ \tau_{\theta z} &= \frac{\mu}{r}\frac{\partial w^*}{\partial \theta}, \end{aligned} \tag{2}$$

where μ is the shear modulus of elasticity of the material.

Substituting Equation (2) into Equation (1) yields the wave equation represented by the displacement as:

$$\nabla^2 w^* - \frac{1}{c^2}\frac{\partial^2 w^*}{\partial t^2} = 0, \tag{3}$$

where $\nabla^2 = \frac{\partial^2}{\partial r^2} + \frac{1}{r}\frac{\partial}{\partial r} + \frac{1}{r^2}\frac{\partial^2}{\partial \theta^2}$ is the Laplacian operator. $c = \sqrt{\mu/\rho}$ is the wave velocity.

Taking the Fourier transform of Equation (3), we achieve:

$$\nabla^2 \int_{-\infty}^{+\infty} w^* \mathrm{e}^{-\mathrm{i}\omega t} dt - \frac{1}{c^2} \int_{-\infty}^{+\infty} \frac{\partial^2 w^*}{\partial t^2} \mathrm{e}^{-\mathrm{i}\omega t} dt = 0. \tag{4}$$

Letting $\varphi(r,\theta,\omega) = \int_{-\infty}^{+\infty} w^* \mathrm{e}^{-\mathrm{i}\omega t} dt$ and $w^*(r,\theta,t) = \frac{1}{2\pi} \int_{-\infty}^{+\infty} \varphi(r,\theta,\omega) \mathrm{e}^{\mathrm{i}\omega t} d\omega$, we obtain the Helmholtz equation as:

$$\nabla^2 \varphi + k^2 \varphi = 0, \tag{5}$$

where $k = \omega/c$ is the wave number, $\varphi(r, \theta, \omega)$ is the spectral function of $w^*(r, \theta, t)$, and Equation (5) is the Helmholtz equation satisfied by $\varphi(r, \theta, \omega)$.

3. Incident Waves and Scattered Waves

Assuming that the generation time of the SH wave is T, the wave field of the incident wave at time interval $t \leq 0$ is represented as $w^{(i)} = 0$. Therefore, based on the properties of the incident wave, the wave field function is transformed into an odd function with a period of 2T using odd extension. As shown in Figure 1, the SH wave is incident from the right. Furthermore, by expanding the Fourier series, the wave field of the incident wave can be expressed as the superposition of sine waves with different frequencies and amplitudes, with the result:

$$w^{(i)} = \sum_{n=1}^{\infty} a_n \sin\left(n\omega_0 \frac{r}{c} \cos\theta - n\omega_0 t \right), \tag{6}$$

where a_n is the harmonic amplitude coefficient, $\omega_0 = \pi/\mathrm{T}$ is the fundamental frequency, and t is the wave field response time.

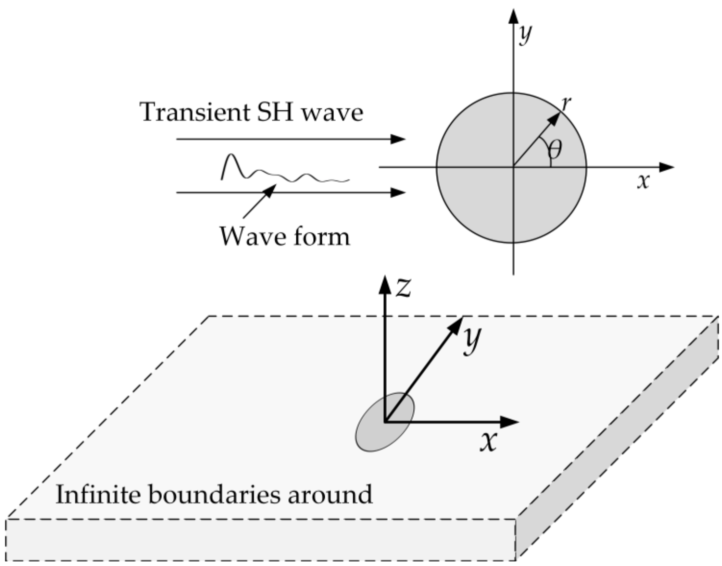

Figure 1. Schematic diagram of SH wave incident.

Equation (6) is rewritten in complex exponential form as [11]:

$$w^{(i)} = \sum_{n=0}^{\infty} a_n \mathrm{e}^{\mathrm{i}\left(n\omega_0 \frac{r}{c} \cos\theta - n\omega_0 t\right)}, \tag{7}$$

where the imaginary part of $w^{(i)}$ represents the actual displacement of the particle.

The Fourier transform of Equation (7) can be expressed as:

$$\varphi^{(i)}(r,\theta,\omega) = 2\pi \sum_{n=1}^{\infty} a_n \delta(\omega + n\omega_0) \mathrm{e}^{-\mathrm{i}kr\cos\theta}. \tag{8}$$

Using the wave function expansion method, Equation (7) is expressed as [4]:

$$w^{(i)} = \sum_{n=1}^{\infty} \left[a_n \mathrm{e}^{-\mathrm{i}n\omega_0 t} \sum_{m=0}^{+\infty} \mathrm{i}^m \varepsilon_m J_m(\frac{n\omega_0 r}{c}) \cos m\theta \right]. \tag{9}$$

The wave field of the scattered wave generated by the circular opening can be written as [4]:

$$w^{(s)} = \sum_{n=1}^{\infty} \left[a_n \mathrm{e}^{-\mathrm{i}n\omega_0 t} \sum_{m=0}^{+\infty} A_m H_m^{(1)}(\frac{n\omega_0 r}{c}) \cos m\theta \right], \tag{10}$$

where $J_m(\cdot)$ represents the first kind Bessel function, and $H_m^{(1)}(\cdot)$ represents the first kind Hankel function.

Then, the total elastic field can be expressed as:

$$w^{(t)} = w^{(i)} + w^{(s)}. \tag{11}$$

By substituting Equations (9) and (10) into Equation (2), the shear stress generated by the wave field of the incident wave can be obtained, and the result is:

$$\tau_{rz}^{(i)} = \mu \sum_{n=1}^{\infty} \frac{n\omega_0}{2c} \left\{ a_n \mathrm{e}^{-\mathrm{i}n\omega_0 t} \sum_{m=0}^{\infty} \mathrm{i}^m \varepsilon_m \left[J_{m-1}(\frac{n\omega_0 r}{c}) - J_{m+1}(\frac{n\omega_0 r}{c}) \right] \cos m\theta \right\}, \tag{12}$$

$$\tau_{\theta z}^{(i)} = \frac{\mu}{r} \sum_{n=1}^{\infty} \left[a_n \mathrm{e}^{-\mathrm{i}n\omega_0 t} \sum_{m=0}^{\infty} \mathrm{i}^m \varepsilon_m J_m(\frac{n\omega_0 r}{c}) m \sin m\theta \right]. \tag{13}$$

Simultaneously, the scattered wave generated by an irregular opening can be expressed as:

$$\tau_{rz}^{(s)} = \mu \sum_{n=1}^{\infty} \frac{n\omega_0}{2c} \left\{ a_n \mathrm{e}^{-\mathrm{i}n\omega_0 t} \sum_{m=0}^{\infty} A_m \left[H_{m-1}^{(1)}(\frac{n\omega_0 r}{c}) - H_{m+1}^{(1)}(\frac{n\omega_0 r}{c}) \right] \cos m\theta \right\}, \tag{14}$$

$$\tau_{\theta z}^{(i)} = \frac{\mu}{r} \sum_{n=1}^{\infty} \left[a_n \mathrm{e}^{-\mathrm{i}n\omega_0 t} \sum_{m=0}^{\infty} A_m H_m^{(1)}(\frac{n\omega_0 r}{c}) m \sin m\theta \right]. \tag{15}$$

Therefore, the dynamic stress around the circular opening can be expressed as:

$$\tau_{rz}^{(t)} = \tau_{rz}^{(i)} + \tau_{rz}^{(s)} = \frac{\mu\omega_0}{2c} \sum_{n=1}^{\infty} \tau_{rz}^{(n)}, \tag{16}$$

$$\tau_{\theta z}^{(t)} = \tau_{\theta z}^{(i)} + \tau_{\theta z}^{(s)} = \frac{\mu}{r} \sum_{n=1}^{\infty} \tau_{\theta z}^{(n)}, \tag{17}$$

where

$$\begin{aligned}
\tau_{rz}^{(n)} \quad &= n a_n \mathrm{e}^{-\mathrm{i}n\omega_0 t} \sum_{m=0}^{\infty} \mathrm{i}^m \varepsilon_m \left[J_{m-1}(\tfrac{n\omega_0 r}{c}) - J_{m+1}(\tfrac{n\omega_0 r}{c}) \right] \cos m\theta \\
&+ n a_n \mathrm{e}^{-\mathrm{i}n\omega_0 t} \sum_{m=0}^{\infty} A_m \left[H_{m-1}^{(1)}(\tfrac{n\omega_0 r}{c}) - H_{m+1}^{(1)}(\tfrac{n\omega_0 r}{c}) \right] \cos m\theta, \\
\tau_{\theta z}^{(n)} \quad &= a_n \mathrm{e}^{-\mathrm{i}n\omega_0 t} \sum_{m=0}^{\infty} \left[\mathrm{i}^m \varepsilon_m J_m(\tfrac{n\omega_0 r}{c}) + A_m H_m^{(1)}(\tfrac{n\omega_0 r}{c}) \right] m \sin m\theta.
\end{aligned}$$

The relation between the wave field propagation time and the dynamic stress response time around the circular opening is:

$$t' = t - s/c, \tag{18}$$

where t' is the response time of the dynamic stress and s is the vertical distance from the incident position of the wave field to the edge of the circular opening.

Then, the dynamic stress of the circular opening can be expressed by the result after delay, and the result is:

$$\tau_{rz}(t') = \tau_{rz}^{(t)}(t')\prod(t), \tag{19}$$

$$\tau_{\theta z}(t') = \tau_{\theta z}^{(t)}(t')\prod(t), \tag{20}$$

where the rectangle function $\prod(t) = h(t-a) - h(t-a-T)$, $a = \frac{s+r_0(1+\cos\theta)}{c}$. $h(\cdot)$ is the unit step function and $t \in [0, \mathrm{T} + (s+2r_0)/c]$, $t_0 = a + \mathrm{T}/2$.

4. Dynamic Stress Concentration Coefficient and Dynamic Stress Coefficient

In the transient problem, the range of the wave field is considered to be limited only to the vicinity of the circular opening, so that the surrounding boundary can be ignored. The boundary conditions for this problem are

$$\tau_{rz}|_{r=r_0} = 0, \tag{21}$$

where r_0 is the radii of the opening.

The infinite series τ_{rz} is identical to zero in the time period $t \in [0, \mathrm{T} + 2r_0/c]$, requiring every term in the series to be identical to zero, and since cos$m\theta$ is orthogonal for all m in the interval (0, 2π), the coefficient of cos$m\theta$ must be zero. Upon substituting Equation (19) into Equation (21) to obtain undetermined coefficients, the result is:

$$A_m = -\frac{\mathrm{i}^m \varepsilon_m \left[J_{m-1}\left(\frac{n\omega_0 r_0}{c}\right) - J_{m+1}\left(\frac{n\omega_0 r_0}{c}\right)\right]}{H_{m-1}^{(1)}\left(\frac{n\omega_0 r_0}{c}\right) - H_{m+1}^{(1)}\left(\frac{n\omega_0 r_0}{c}\right)}. \tag{22}$$

The dynamic stress of the circular opening can be expressed as the modulus of the imaginary part of the solution, with the following result:

$$\tau_{\theta z}^{*}|_{r=r_0} = |\mathrm{Im}\tau_{rz}| = \frac{\mu}{r_0}\prod(t)\left|\sum_{n=1}^{\infty}\mathrm{Im}\tau_{\theta z}^{(n)}\right|. \tag{23}$$

The dynamic stress component of the elastic field can be expressed as a separation of time and space variables, with the result:

$$\tau_{\theta z}^{(n)}(r,\theta,t') = \tau_{\theta z}^{(n)}(r,\theta)T^{(n)}(t'), \tag{24}$$

where $\tau_{\theta z}^{(n)}(r,\theta)$ is a space function and $T^{(n)}(t')$ is a time function, and the imaginary part of their product is the actual dynamic stress.

By substituting Equation (17) into Equation (24), we obtain:

$$\tau_{\theta z}^{(n)}(r,\theta) = \left[\mathrm{i}^m \varepsilon_m J_m\left(\frac{n\omega_0 r}{c}\right) + A_m H_m^{(1)}\left(\frac{n\omega_0 r}{c}\right)\right] m \sin m\theta, \tag{25}$$

$$T^{(n)}(t') = a_n \mathrm{e}^{-\mathrm{i}n\omega_0 t'}. \tag{26}$$

The space function $\tau_{\theta z}^{(n)}(r,\theta)$ can be written in the following form:

$$\tau_{\theta z}^{(n)}(r,\theta) = C_n + \mathrm{i}D_n, \tag{27}$$

where C_n and D_n are the real and imaginary parts of $\tau_{\theta z}^{(n)}(r,\theta)$.

Substituting Equations (26) and (27) into Equation (23), we can obtain:

$$\tau_{\theta z}^{*}(r,\theta,t')\big|_{r=r_0} = \frac{\mu}{r_0}\prod(t)\left|\sum_{n=1}^{\infty} E_n(\theta)\sin[n\omega_0 t' - \phi_n(\theta)]\right|, \quad (28)$$

where $E_n(\theta) = -a_n\sqrt{C_n^2 + D_n^2}$, $\phi_n(\theta) = \arctan(C_n/D_n)$.

Using complex variable $\zeta = \theta + \mathrm{i}t$, $\overline{\zeta} = \theta + \mathrm{i}t$, assume that the opening edge stress is

$$\tau_{\theta z}^{*}(r_0,\theta_j,t_j) = \frac{\mu}{r_0}\prod(t_j)\sum_{n=1}^{\infty}\left|E_n(\theta_j)\sin[n\omega_0 t_j - \phi_n(\theta_j)]\right|. \quad (29)$$

The DSCC can then be defined as [14]:

$$DSCC = \left|\frac{\tau_{\theta z}^{*}(\zeta)}{\tau_0}\right|, \quad (30)$$

where $\tau_0 = \max\left(\tau_{\theta z}^{(i)}\right)$ represents the maximum stress generated by incident wave $\tau_{\theta z}^{(i)}$.

5. Numerical Examples and Discussion

From the convergence of the Bessel function, it can be seen that when $m \geq \mathrm{M}$, the space function $\tau_{\theta z}^{(n)}(r,\theta)$ can converge. After many calculations, the calculation accuracy can meet the requirements when m = 20. Using the common material 16NiCr4 in industry as an example, its density is $\rho = 7.8 \times 10^3$ kg·m^{-3} and its shear modulus is $\mu = 7.9 \times 10^{10}$ N·m^{-2}.

The characteristics of SH wave incidence are as follows: (i) the impact time of incident wave is short, and the response time of circular opening is generally 5~20 ms and (ii) the frequency of the incident wave is high and the frequency band is wide, generally 50~1000 Hz. Considering that the distance from the wave source to the edge of the opening is s = 0, the spectral function of SH wave in the example $\varphi^{(i)}(r, \theta, \omega)$ is given in Table 1, where n = 10, circular frequency $\omega_0 = 100\pi$, and harmonic amplitude coefficient $a_\mathrm{n} \in (0, 0.2)$ mm. The waveform diagram corresponding to the spectral function in the time domain is shown in Figure 2.

Table 1. Spectrum function of periodic shockwave.

ω	ω_0	$2\omega_0$	$3\omega_0$	$4\omega_0$	$5\omega_0$	$6\omega_0$	$7\omega_0$	$8\omega_0$	$9\omega_0$	$10\omega_0$
a_n/mm	1.66	1.64	1.14	1.14	0.572	1.40	1.60	0.883	0.892	0.931

Figure 2 shows the temporal distribution of the wavefield generated by the incident wave. At time T = 10 ms, the wavefield is fully established. The maximum displacement occurs at time t = 0.71 ms, with a value of a = 0.86 mm. Initially, the displacement undergoes significant variations, indicating a rapid change in the amplitude of the wavefield during this time interval. After approximately t = 2 ms, the displacement exhibits more minor variations. It gradually decreases to zero at time t = T. This signifies a gradual decrease in the amplitude of the wavefield until it eventually vanishes. This temporal behavior of the wavefield provides insights into the incident wave's dynamic response and propagation characteristics.

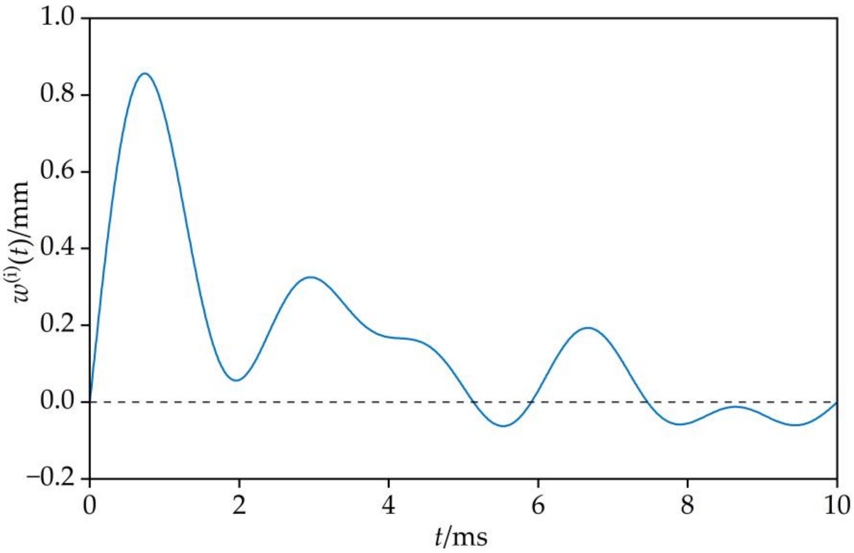

Figure 2. Time domain waveform of transient SH wave incident wave.

Based on the data presented in Figure 3, we can observe the temporal variation of the time stress peak coefficient (TSPC) peak at different radii. The TSPC consists of the maximum value of the DSCC at each moment. For a radius of 1, the peak of TSPC reaches 2.27, corresponding to a time of 0.44 ms. Similarly, at a radius of 2, the peak of TSPC is 1.75, occurring at 1.11 ms. In the case of a radius of 3, the peak of TSPC is 1.41, with a corresponding time of 1.08 ms. From the figure, it can be observed that peaks are predominantly concentrated in the initial transient response, indicating that the maximum value of TSPC is achieved during the initial stages of the system. Subsequently, after exceeding 2 ms, the amplitude of TSPC significantly attenuates. This observation is consistent with the temporal waveform figure in Figure 2, further reinforcing this relationship. These findings are essential for understanding the system's dynamic behavior and identifying appropriate parameter configurations and optimization control strategies.

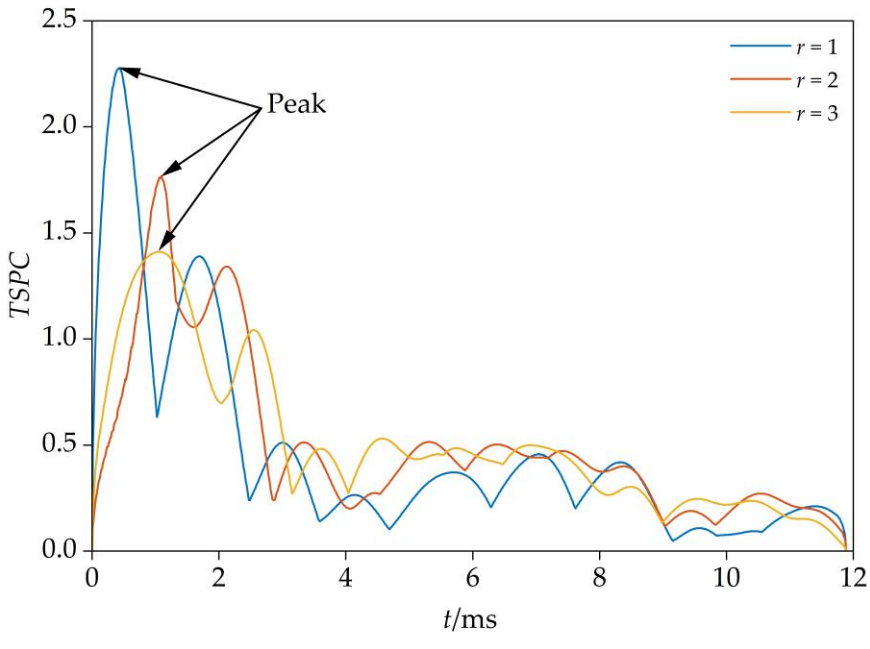

Figure 3. Change of TSPC with time at different radii, r = 1, 2, 3.

The opening edge DSCC corresponding to the peak of each curve in Figure 3 is shown in Figure 4. It is evident from the figure that each curve is not complete, indicating that the

TSPC only exists during the initial stage of shockwave impact. Specifically, when the radius of the opening is 1, the stress response at the opening edge is significantly greater than when the opening radii are 2 and 3. This suggests that, under a constant incident wave, the smaller the aperture, the higher the peak of DSCC generated at the opening edge. This observation highlights the influence of the size of the aperture on the stress concentration phenomenon during shockwave impact.

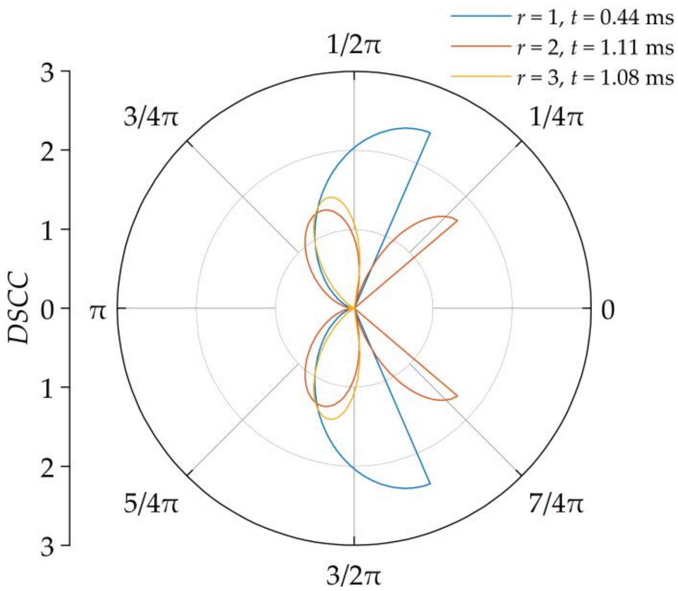

Figure 4. Opening edge DSCC corresponding to peak time with r = 1, 2, 3.

Figure 5 illustrates the distribution of the position peak stress coefficient (PSPC) at the edge of the opening with changes in position. From the observations in Figure 5, it can be seen that as the aperture size increases, the distribution of PSPC gradually shifts toward the shaded region, and the range of PSPC also narrows. These findings further support the conclusion that smaller apertures correspond to greater dynamic stress concentrations. As the aperture size increases, the restrictions on the shockwave passing through the opening diminish. This restriction reduction decreases the stress concentration area near the aperture edge, causing the PSPC distribution to shift progressively toward the shaded region. Additionally, the range of PSPC also gradually narrows as the aperture size increases. This narrowing range may be attributed to the larger aperture, resulting in a more uniform stress distribution. Overall, these observations highlight the influence of aperture size on the distribution of PSPC and provide further insights into the dynamic stress concentration phenomenon.

Figure 6 shows the peak value of the DSCC and its occurrence as the r_0 changes. It can be observed that the peak value of the DSCC displays continuous variations in its numerical value and limits toward a constant. In terms of location, the peak is primarily concentrated at the upper and lower ends of the circular opening, specifically at $\theta = \pi/2$ and $3\pi/2$. The discontinuity of the DSCC peak at the opening edge may be attributed to changes in sidelobes. However, as the radius increases, the location of the peak gradually stabilizes.

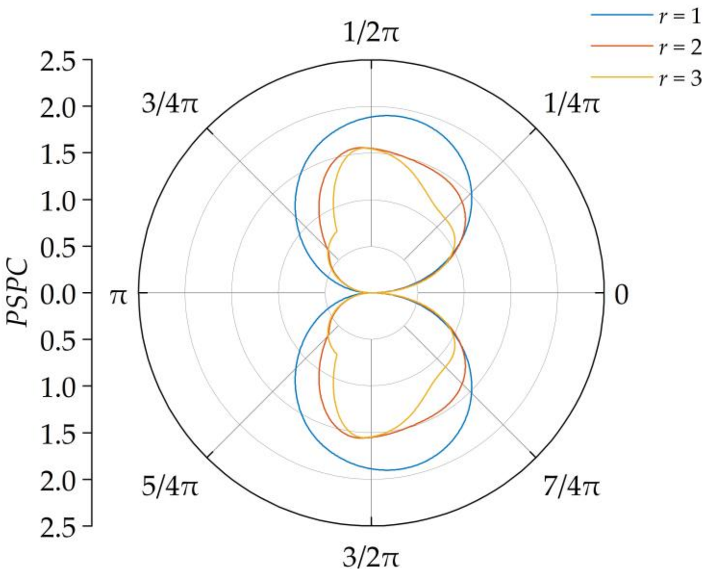

Figure 5. The distribution of the PSPC at the edge of the opening with changes in position with $r = 1, 2, 3$.

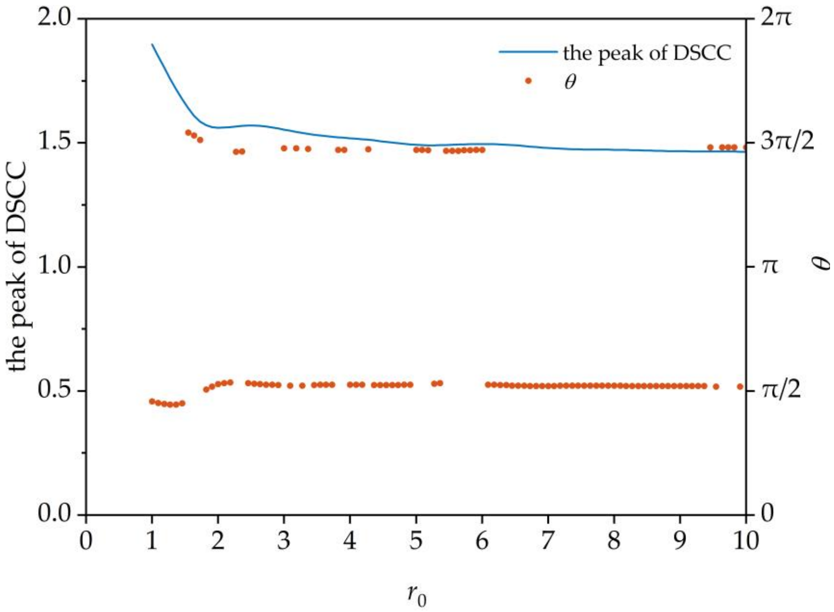

Figure 6. The peak value of the DSCC and its occurrence as the r_0 changes.

Figures 7 and 8 depict the variations of the DSCC under different aperture sizes and angles. When the aperture size is small ($r = 1$), the range of DSCC variation is also limited as the detection position transitions from the shaded region to the illuminated region, and the curve representing the change in DSCC shifts toward the left in the figure. This indicates that the DSCC decreases as the detection position moves from the shaded region to the illuminated region. However, in the case of a large aperture, the initial value of the shaded region is opposite to that of the illuminated region. This means the DSCC increases as the detection position moves from the shaded region to the illuminated region. This behavior differs from a small aperture, where the DSCC decreases as the detection position moves from the shaded region to the illuminated region. These observations highlight the influence of both aperture size and detection position on the variation of DSCC.

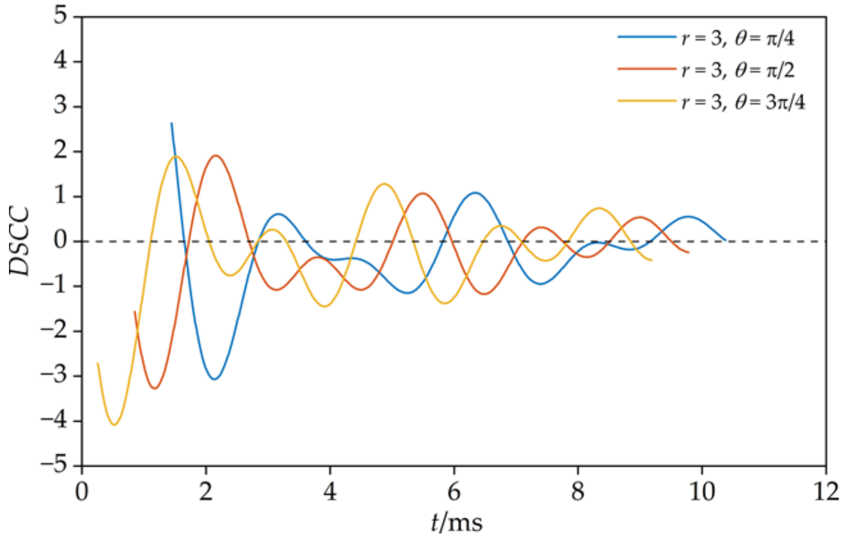

Figure 7. Change of DSCC over time at different positions with $r = 3$.

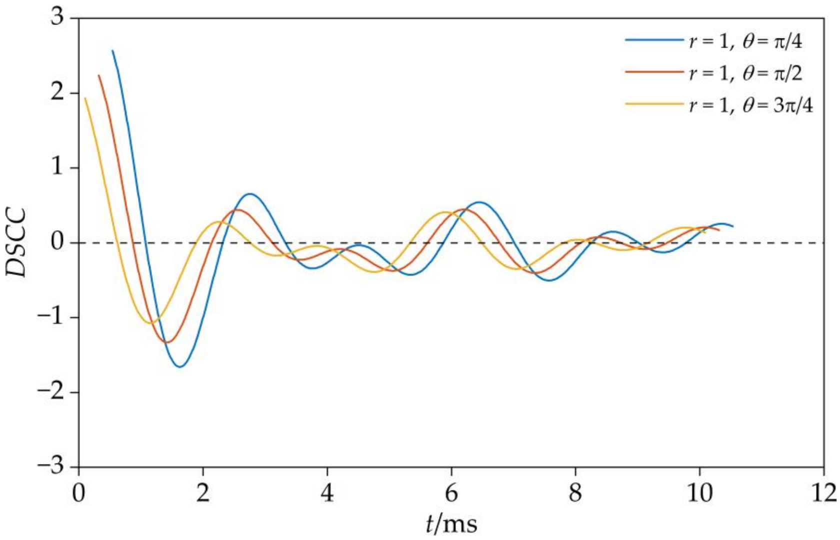

Figure 8. Change of DSCC over time at different positions with $r = 1$.

Figure 9 shows the nephogram of DSCC over time along the edge in the range 0 to π. In the figure, the radius of the aperture of the circle is 1. At each moment, the distribution of DSCC is mainly concentrated around the $\pi/2$ position. In terms of position change, DSCC increases first and then decreases. In terms of time, the change of DSCC is consistent with the change of incident wave. These observations provide insights into the temporal and positional dynamics of the DSCC.

Figure 10 shows the distribution of stress peak coefficients in time and space. It can be observed that the stress peak coefficient exhibits spatial symmetry concerning the circular aperture and is mainly concentrated in the light region. Regarding time, stress peak coefficient is concentrated in the 0–4.61 ms range. The higher stress peak coefficient (SPC) values are concentrated in two regions: $\pi/4$–$\pi/2$ and $3\pi/2$–$7\pi/4$.

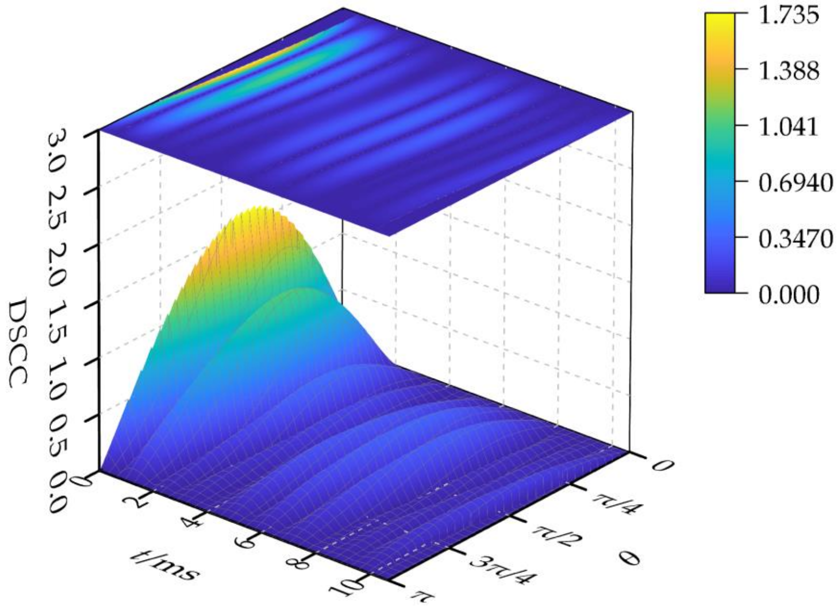

Figure 9. The nephogram of DSCC overtime at the opening edge with the range (0, π).

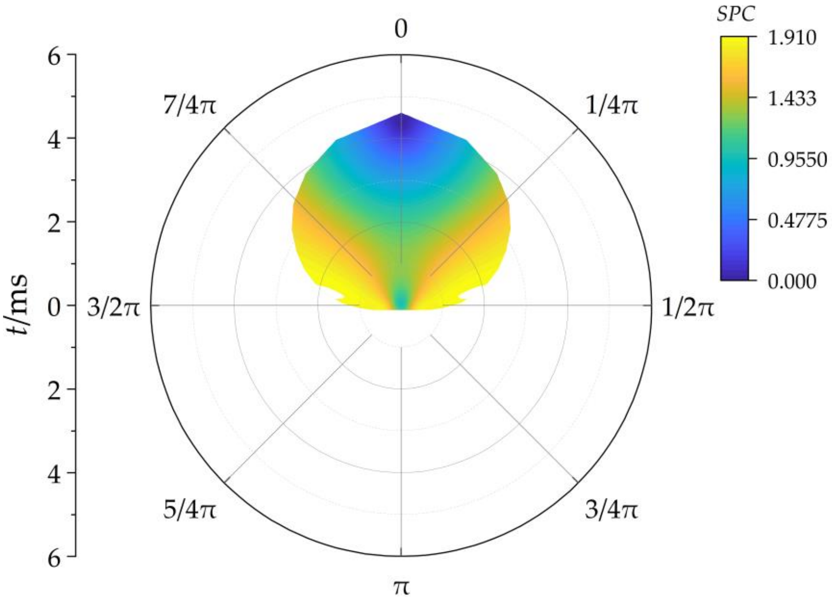

Figure 10. Spatial and temporal distribution of stress peak coefficient with $r = 1$.

6. Conclusions

This study investigates the transient response of stress fields in circular apertures. The innovation of this paper is that a multi-frequency SH wave incident simulation method is proposed to simulate the impact scene, and the transient response of the circular opening stress field is investigated by simplifying the technique and using Fourier transform. Remarkably, considering the causal nature of both the wave field and the response, a rectangular function represents the temporal delay. This method can play an important role in seismic design, mineral exploration, nondestructive testing, blasting, and the application and progress of advanced composite materials.

Considering the complexity of the DSCC expression, a theoretical calculation is performed using the wave function expansion method. The superposition of Bessel and Hankel functions represents displacement and stress. The undetermined coefficients can be determined by applying the boundary conditions associated with the circular aperture.

This strategy provides a solution for addressing similar challenges. The method presented in this paper is suitable for large boundary materials with circular openings. Materials with complex defects and boundaries need further investigation.

More details can be obtained from numerical results:

1. The radii of the circular opening significantly impact the DSCC. It is crucial to consider the dynamic stress concentration at the opening when designing structures or assessing the strength of materials.
2. The stress peak coefficient is primarily concentrated in the initial transient response in the light region. Therefore, when designing materials with openings in a multi-vibration environment, it is essential to consider and account for the maximum impact during the transient response.
3. As the radii of the circular opening increase, the sidelobe of the DSCC appears earlier. This means that the opening is subjected to alternating stress at an earlier stage, which can lead to fatigue damage. It is essential to consider the effects of alternating stress and fatigue when designing structures with larger circular openings.

Author Contributions: Conceptualization, Z.W. and C.Z.; methodology, J.W.; validation, R.L., R.Z. and Y.G.; formal analysis, W.P.; investigation, J.W. and R.L.; data curation, W.P.; writing—original draft preparation, J.W.; writing—review and editing, Z.W.; supervision, Y.G.; project administration, C.Z.; funding acquisition, R.L. and R.Z. All authors have read and agreed to the published version of the manuscript.

Funding: This research was funded by the Sichuan Science and Technology Program (No. 2022YFG0274), National Natural Science Foundation of China (Grant No. 51875146).

Institutional Review Board Statement: Not applicable.

Informed Consent Statement: Not applicable.

Data Availability Statement: The authors confirm that the data supporting the findings of this study are available within the article.

Conflicts of Interest: The authors declare no conflict of interest.

References

1. Isiet, M.; Mišković, I.; Mišković, S. Review of peridynamic modelling of material failure and damage due to impact. *Int. J. Impact Eng.* **2021**, *147*, 103740. [CrossRef]
2. Pao, Y.-H.; Mow, C.-C.; Achenbach, J. Diffraction of elastic waves and dynamic stress concentrations. *J. Appl. Mech.* **1973**, *40*, 872. [CrossRef]
3. Xue, H.; Zhou, C.; Cheng, G.; Bao, J.; Wang, M.; Gong, Y.; Ji, H.; Yang, W.; Hou, B.; Zhou, W. Scattering of Magnetoacoustic Waves and Dynamic Stress Concentration around Double Openings in Piezomagnetic Composites. *Materials* **2021**, *14*, 6878. [CrossRef]
4. Kara, H.F.; Aydogdu, M. Dynamic response of a functionally graded tube embedded in an elastic medium due to SH-Waves. *Compos. Struct.* **2018**, *206*, 22–32. [CrossRef]
5. Leng, J.; Qi, H.; Feng, H.L.; Fan, Z.Y. Dynamic responses of a plate with two circular cavities subjected to SH waves. *Mech. Adv. Mater. Struct.* **2023**, *30*, 4216–4226. [CrossRef]
6. Jiang, G.-X.-X.; Yang, Z.-L.; Sun, C.; Song, Y.-Q.; Yang, Y. Analytical study of SH wave scattering by a cylindrical cavity in the two-dimensional and approximately linear inhomogeneous medium. *Waves Random Complex Medium* **2020**, *31*, 1799–1817. [CrossRef]
7. Tang, Y.; Zhu, Z.; Ba, Z.; Gong, W. Scattering of shallow asymmetric V-shaped canyon under cylindrical SH waves. *J. Eng. Math.* **2023**, *141*, 7. [CrossRef]
8. An, N.; Song, T.-S. Dynamic fracture behavior for functionally graded piezoelectric bi-materials with interfacial cracks near a circular opening. *Waves Random Complex Medium* **2021**, 1–19. [CrossRef]
9. Jiang, Y.; Zhou, C.; Wang, B.; Wu, L. Magnetoelastic coupled wave diffraction and dynamic stress intensity factor in graded piezomagnetic composites with a cylindrical aperture. *Materials* **2020**, *13*, 669. [CrossRef] [PubMed]
10. Baytak, T.; Bulut, O. Thermal Stress in Functionally Graded Plates with a Gradation of the Coefficient of Thermal Expansion Only. *Exp. Mech.* **2022**, *62*, 655–666. [CrossRef]
11. Zhou, C.; Hu, C.; Ma, F.; Liu, D. Elastic wave scattering and dynamic stress concentrations in exponential graded materials with two elliptic openings. *Wave Motion* **2014**, *51*, 466–475. [CrossRef]

12. Kumar, H.S.N.; Kattimani, S.; Nguyen-Thoi, T. Influence of porosity distribution on nonlinear free vibration and transient responses of porous functionally graded skew plates. *Def. Technol.* **2021**, *17*, 1918–1935. [CrossRef]
13. An, N.; Song, T.; Hou, G. Dynamic performance for piezoelectric bi-materials with an interfacial crack near an eccentric elliptical opening under anti-plane shearing. *Math. Mech. Solids* **2021**, *27*, 93–107. [CrossRef]
14. Zhao, M.; Song, T.-s.; An, N.; Hou, G. Dynamic anti-plane behavior for a semi-infinite piezoelectric medium with a locally debonded cylindrical inclusion near the surface. *AIP Adv.* **2020**, *10*, 075323. [CrossRef]
15. Jiang, G.; Yang, Z.; Sun, C.; Li, X.; Yang, Y. Dynamic stress concentration of a cylindrical cavity in vertical exponentially inhomogeneous half space under SH wave. *Meccanica* **2019**, *54*, 2411–2420. [CrossRef]
16. Jiang, G.; Yang, Z.; Sun, C.; Sun, B.; Yang, Y. Dynamic response of a circular inclusion embedded in inhomogeneous half-space. *Arch. Appl. Mech.* **2018**, *88*, 1791–1803. [CrossRef]
17. Yang, Z.; Bian, J.; Song, Y.; Yang, Y.; Sun, M.H. Scattering of cylindrical inclusions in half space with inhomogeneous shear modulus due to SH wave. *Arch. Appl. Mech.* **2021**, *91*, 3449–3461. [CrossRef]
18. Xiang, M.; Qi, H.; Guo, J. Scattering of SH guided wave by a circular cavity in a strip with the serrated boundary. *Waves Random Complex Medium* **2022**, *32*, 1551–1570. [CrossRef]
19. Panji, M.; Ansari, B. Transient SH-wave scattering by the lined tunnels embedded in an elastic half-plane. *Eng. Anal. Bound. Elem.* **2017**, *84*, 220–230. [CrossRef]
20. Panji, M.; Mojtabazadeh-Hasanlouei, S. Surface Motion of Alluvial Valleys Subjected to Obliquely Incident Plane SH-Wave Propagation. *J. Earthq. Eng.* **2022**, *26*, 6352–6377. [CrossRef]
21. Zhou, X.; Shui, G.S. Transient waves in a piezomagnetic half-space subjected to dynamic anti-plane loading. *Waves Random Complex Medium* **2022**, 1–29. [CrossRef]
22. Tao, M.; Ma, A.; Cao, W.; Li, X.; Gong, F. Dynamic response of pre-stressed rock with a circular cavity subject to transient loading. *Int. J. Rock Mech. Min. Sci.* **2017**, *99*, 1–8. [CrossRef]
23. Shi, W.Z.; Chen, W.W.; Lu, C.; Chen, Y. Interaction of circumferential SH0 guided wave with circumferential cracks in pipelines. *Nondestr. Test. Eval.* **2021**, *36*, 571–596. [CrossRef]